29. Messenger, S., Keller, L. P., Stadermann, F. J., Walker, R. M. & Zinner, E. Samples of stars beyond the solar system: Silicate grains in interplanetary dust. *Science* **300,** 105–108 (2003).
30. Nagashima, K., Krot, A. N. & Yurimoto, H. Stardust silicates from primitive meteorites. *Nature* **428,** 921–924 (2004).

Supplementary Information accompanies the paper on **www.nature.com/nature**.

Acknowledgements Samples were provided by NASA. We thank J. Aléon, G. Libourel, B. Marty, A. Pack, F. Robert and Z. Sharp for discussions, B. Marty for encouragement, and K. Terada for help in sample preparation. This study was supported by the Mitsubishi Foundation, JSPS, MEXT, Région Lorraine, CNES-CSEEM and by INSU-PNP through a 'Poste Rouge' fellowship (K.H.).

Competing interests statement The authors declare that they have no competing financial interests.

Correspondence and requests for materials should be addressed to K.H. (kohash@ess.sci.osaka-u.ac.jp).

Unconventional superconductivity in $PuCoGa_5$

N. J. Curro[1], T. Caldwell[1], E. D. Bauer[1], L. A. Morales[1], M. J. Graf[1], Y. Bang[2], A. V. Balatsky[1], J. D. Thompson[1] & J. L. Sarrao[1]

[1]*Los Alamos National Laboratory, Los Alamos, New Mexico 87545, USA*
[2]*Department of Physics, Chonnam National University, Kwangju 500-757, Korea*

In the Bardeen–Cooper–Schrieffer theory of superconductivity, electrons form (Cooper) pairs through an interaction mediated by vibrations in the underlying crystal structure. Like lattice vibrations, antiferromagnetic fluctuations can also produce an attractive interaction creating Cooper pairs, though with spin and angular momentum properties different from those of conventional superconductors. Such interactions have been implicated for two disparate classes of materials—the copper oxides[1,2] and a set of Ce- and U-based compounds[3]. But because their transition temperatures differ by nearly two orders of magnitude, this raises the question of whether a common pairing mechanism applies. $PuCoGa_5$ has a transition temperature intermediate between those classes and therefore may bridge these extremes[4]. Here we report measurements of the nuclear spin-lattice relaxation rate and Knight shift in $PuCoGa_5$, which demonstrate that it is an unconventional superconductor with properties as expected for antiferromagnetically mediated superconductivity. Scaling of the relaxation rates among all of these materials (a feature not exhibited by their Knight shifts) establishes antiferromagnetic fluctuations as a likely mechanism for their unconventional superconductivity and suggests that related classes of exotic superconductors may yet be discovered.

Cooper pairs, which have zero net spin and angular momenta in conventional superconductors, condense into a macroscopic quantum state that is separated energetically from all unpaired electrons by a finite gap Δ. Because of this gap, measurements that probe the electronic density of states near the Fermi energy exhibit a thermally activated temperature dependence below the superconducting transition temperature T_c. On the other hand, Cooper pairs formed by the exchange of antiferromagnetic spin fluctuations possess even parity and non-zero angular momentum[5]; consequently, the superconducting energy gap is not finite everywhere but vanishes at points or along lines in momentum space. These gap nodes have a profound influence on the properties observed at low temperature. For any finite temperature, well-defined electronic excitations or quasiparticles reside at these nodes, and measurements sensitive to the electronic density of states exhibit power-law variations with temperature that depend solely on the topology of the gap zeros.

The high-T_c copper oxides and certain Ce- and U-based compounds, called heavy-fermion materials, have unconventional, nodal superconducting gaps and support antiferromagnetic fluctuations that lead naturally to these gap structures. These fluctuations common to both classes of materials are a consequence of strong electron–electron correlations: both the *d*-electrons in the copper oxides and the *f*-electrons in the heavy fermion materials experience strong on-site Coulomb repulsion that introduces elements of both localized and itinerant behaviour. In the *d*-electron materials these correlations create a Mott insulator in the undoped case and in the *f*-electron systems lead to enhanced effective electron mass. $PuCoGa_5$ crystallizes in exactly the same structure as does one of these unconventional, heavy-fermion superconductors: $CeCoIn_5$. Their common crystal structure and similarities of magnetic properties derived from nearly localized *f*-electrons suggest that $PuCoGa_5$ may also be an unconventional superconductor. However, the T_c of $PuCoGa_5$ is nearly an order of magnitude higher than that of $CeCoIn_5$ ($T_c = 2.3$ K, the highest T_c among heavy-fermion systems)[6], but comparable to that of many conventional superconductors, such as Nb_3Sn ($T_c \approx 18$ K). Without a direct probe of the gap symmetry of $PuCoGa_5$ it has been impossible to differentiate conclusively between these two scenarios.

Nuclear magnetic resonance (NMR) and nuclear quadrupolar resonance (NQR) are powerful techniques used to make this distinction[7–12]. Both techniques probe the density of quasiparticle excitations, $N(E)$, with excitation energy E above the Fermi energy, and reveal information about the spin state of the Cooper pairs and the pairing symmetry of the gap function in momentum space, $\Delta(\mathbf{k})$. We have used NMR and NQR to measure the Knight shift, K_s, and the nuclear spin-lattice relaxation rate, T_1^{-1}, of the ^{59}Co and ^{69,71}Ga nuclei in the normal and superconducting states of two samples of $PuCoGa_5$. Figure 1a shows a series of ^{71}Ga NMR spectra obtained from Sample A (see Methods) from which the total Knight shift K_{tot} is determined straightforwardly. Similar data were collected from ^{59}Co NMR (not shown). The temperature dependence of these shifts, plotted in Fig. 1c, reveals a pronounced drop in K_{tot} of both ^{71}Ga and ^{59}Co nuclei at T_c. In the normal states

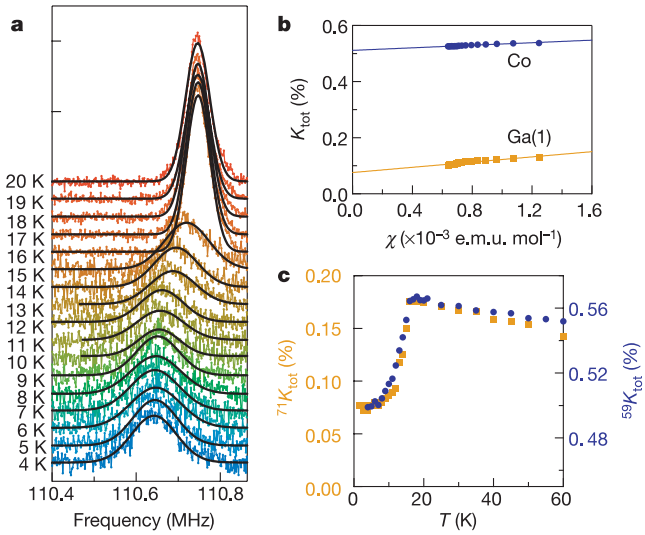

Figure 1 Knight shift measurements in $PuCoGa_5$. **a**, NMR spectra of ^{71}Ga in 8 T at a series of temperatures through T_c. The spectra have been offset vertically for clarity. Solid lines are gaussian fits. **b**, The normal-state magnetic shift K_{tot} of the ^{59}Co and ^{71}Ga(1) versus bulk susceptibility χ. The intercepts and hyperfine constants are given by $^{59}K_{orb} = 0.53\%$, $^{71}K_{orb} = 0.088\%$, and $^{59}A = 1.5$ kOe μ_B^{-1}, $^{71}A = 4.1$ kOe μ_B^{-1}. Solid lines are fits to the low-temperature data. **c**, The total magnetic shift K_{tot} of the ^{59}Co and ^{71}Ga(1) versus temperature.

of metals like $PuCoGa_5$, K_{tot} is the sum of two contributions: $K_{tot} = K_{orb} + K_s$, where K_{orb} is temperature-independent, and $K_s = A\chi_s$, where A is a hyperfine constant, and χ_s is the spin susceptibility. The constants A and K_{orb} were determined independently for ^{59}Co and ^{71}Ga nuclei above T_c, as shown in Fig. 1b. Quantitatively accounting for both K_{orb} and the demagnetization field in the superconducting state, we obtain the temperature dependence of χ_s shown in Fig. 2.

In the superconducting state, χ_s probes the spin symmetry of the Cooper pair wavefunction. When two quasiparticles with up- and down-spin form a Cooper pair with total spin of either $S = 0$ or $S = 1$, the wavefunction is either antisymmetric (spin-singlet or more generally even-parity) or symmetric (spin-triplet or odd-parity) under particle exchange. For singlet pairing, χ_s decreases in the superconducting state, but for triplet pairing χ_s remains constant (depending on the orientation of the applied magnetic field[12]). The decrease evident in Fig. 2 clearly establishes $PuCoGa_5$ as a spin-singlet superconductor. To satisfy Fermi statistics, the pair wavefunction must be antisymmetric with respect to particle exchange. Because the spin part of the wavefunction is antisymmetric (singlet), the symmetry of the orbital component of the wavefunction (given by $(-1)^L$, where the angular momentum $L = 0, 1, 2, 3, \ldots$ or $s, p, d, f, \ldots$) must be symmetric, so L must be even. Thus, the results of Fig. 2 leave open the possibility that $PuCoGa_5$ could be either a conventional s-wave or an unconventional superconductor with $L > 0$ and even.

Although χ_s drops below T_c, as expected for spin-singlet pairing, it should approach zero as $T \rightarrow 0$ (neglecting minor vortex core contributions). In an unconventional, nodal superconductor, impurity scattering creates excitations in the superconducting gap nodes, and hence a finite spin susceptibility. Impurity scattering in $PuCoGa_5$ is inevitable owing to lattice defects created by the recoil of uranium atoms during the radioactive decay of the plutonium, for example, $^{239}Pu \rightarrow {}^{235}U + \alpha$-particle[13]. The solid curve in Fig. 2, discussed below, shows that the temperature dependence of χ_s is described well by calculations that account for impurity scattering in a d-wave superconductor.

Further evidence for nodal superconductivity is provided by spin-lattice relaxation rate measurements on Sample B (see Methods). T_1^{-1} measures the rate at which a nucleus reaches an equilibrium spin temperature; it is dominated by scattering between the conduction electrons and the nuclear spins. In the superconducting state, the condensate cannot relax the nuclei without breaking Cooper pairs, so the nuclei are predominantly relaxed by quasiparticles. Because the symmetry of the orbital part of the Cooper pair wavefunction determines the energy dependence of $N(E)$ below the energy gap Δ, T_1^{-1} establishes the pairing symmetry. The data are shown in Fig. 3a. Below T_c, T_1^{-1} exhibits a sharp decrease, with roughly $T_1^{-1} \propto T^3$ behaviour, followed by $T_1^{-1} \propto T$ at the lowest temperatures. In contrast to expectations for an s-wave superconductor, the lack of a (Hebel–Slichter coherence) peak in T_1^{-1} just below T_c and the power-law dependence of T_1^{-1} are identical to responses found in the copper oxide superconductors and $CeCoIn_5$ (refs 14, 15). Furthermore, the temperature dependence of T_1^{-1} in the normal state of $PuCoGa_5$ is qualitatively different than that observed in conventional BCS superconductors

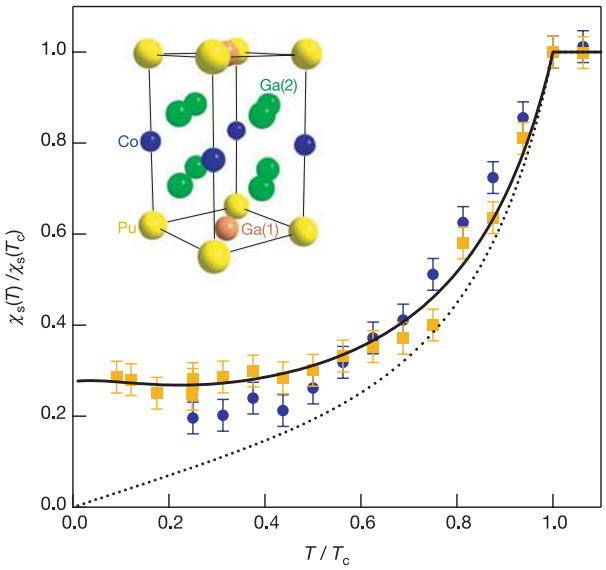

Figure 2 Normalized spin susceptibility in the superconducting state. The ^{59}Co (blue circles) and ^{71}Ga(1) (orange squares) data as well as calculations for pure d-wave (dotted line) and dirty d-wave (solid line) gap functions are shown. The latter assumes strong impurity scattering in the self-consistent T-matrix approximation (SCTA) with scattering rate $\Gamma^A/\Delta = 0.03$, gap $\Delta/k_BT_c = 4$ and $b = 1.74$. Inset, the $PuCoGa_5$ crystal structure, with the Ga site index.

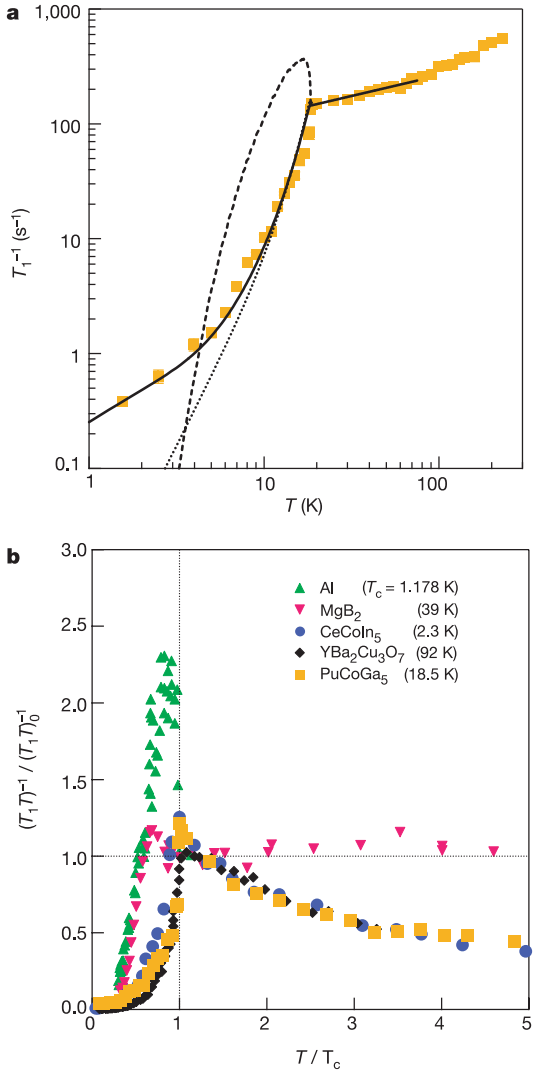

Figure 3 The spin-lattice relaxation rate in the normal and superconducting states. **a**, T_1^{-1} data for the ^{69}Ga(1), as well as calculations for BCS isotropic s-wave (dashed), pure (dotted) and dirty (solid) d-wave gap functions. The solid line in the normal state shows $T^{0.35}$. **b**, $(T_1T)^{-1}/(T_1T)_0^{-1}$ versus T/T_c for $PuCoGa_5$, as well as for the unconventional superconductors $YBa_2Cu_3O_7$ ($T_c = 92$ K; ref. 7) and $CeCoIn_5$ ($T_c = 2.3$ K; ref. 27), and the s-wave superconductors Al ($T_c = 1.178$ K; ref. 8) and MgB_2, ($T_c = 39.2$ K; ref. 11). The normalization constant $(T_1T)_0^{-1}$ is given by the value of $(T_1T)^{-1}$ at $1.25T_c$ (see Methods).

(see Fig. 3b), but has been predicted for a relaxation rate dominated by antiferromagnetic spin fluctuations[16]. Further, the normalized relaxation rates of $PuCoGa_5$, high-T_c $YBa_2Cu_3O_7$ and $CeCoIn_5$ scale onto a common curve as a function of the dimensionless parameter T/T_c. Although we have chosen T_c as an easily defined characteristic energy, we also find that, with a spin-fluctuation energy of $T_0 \approx 270$ K for $PuCoGa_5$ (ref. 17), the T_c and T_0 values of $PuCoGa_5$ have the same proportionality observed for several other unconventional superconductors[18] (see Supplementary Fig. 1). The results of Fig. 3b, consequently, argue that $PuCoGa_5$ is indeed a bridge between extreme cases. A priori, we might expect a similar scaling behaviour among the Knight shifts of these materials; however, the long wavelength ($\mathbf{q} = 0$) response in the normal state of these systems is quite different from the finite $\mathbf{q}$ response that dominates the spin lattice relaxation[2] (see Supplementary Fig. 2).

Self-consistency of our results is provided by calculations of the temperature dependence of T_1^{-1} below T_c for sample B and the Knight shift for sample A within the framework of a self-consistent T-matrix approximation (SCTA)[19,20], considering the effects of impurity scattering on both *s*- and *d*-wave pairing scenarios. The T_1^{-1} data are best-fitted (Fig. 3a, solid curve) by a strong-coupling *d*-wave gap function with lines of nodes and the parameters $\Delta/k_BT_c = 4$ and $\Gamma^B/\Delta = 0.01$, where Γ^B is the impurity scattering rate for sample B. This gap value is significantly enhanced relative to the *d*-wave weak-coupling limit $\Delta/k_BT_c = 2.14$ and very similar to that determined for $CeCoIn_5$ (ref. 15). The temperature dependence of χ_s (Fig. 2 data) is fitted using the same gap magnitude, but with $\Gamma^A/\Delta = 0.03$ for sample A. The difference in the impurity lifetime broadening $\Delta\Gamma = \Gamma^A - \Gamma^B$ is due to the age difference and hence impurity scattering in samples A and B. From the Abrikosov–Gorkov relationship[21] $\Delta T_c = (\pi/4)\Delta\Gamma$, this difference ($\Delta\Gamma/\Delta = 0.02$) implies $\Delta T_c = 1.2$ K, in agreement with both the difference in T_c values of the two samples and time-dependent studies of T_c suppression ($dT_c/dt \approx -0.24$ K per month; Jutier, F. *et al.*, unpublished work). From our fits, we estimate $d\Gamma/dt \approx 0.25$ K per month, which implies that $T_{c0} = 19.1$ K for pristine, defect-free $PuCoGa_5$, a value roughly half that of recent theoretical predictions[22].

The total electronic energy calculations for $PuCoGa_5$ and its isostructural neighbour $NpCoGa_5$ predict that both should order antiferromagnetically[23]. As predicted, $NpCoGa_5$ is an antiferromagnet below the Néel temperature $T_N \approx 47$ K (ref. 24), but there is no evidence for long-range magnetic order above 1 K in $PuCoGa_5$ (ref. 25). These calculations neglect the role of many-electron correlations that lead to a nearly magnetic state in Ce- and U-based heavy-fermion systems, which, in the absence of such correlations, would order magnetically. The existence of these correlations is predicted for Pu-based materials[26] and is reflected in $PuCoGa_5$ through its enhanced electronic specific heat coefficient, $\gamma \approx 95$ mJ mol^{-1} K^{-2} (ref. 17). As with the copper oxides and heavy-fermion systems like $CeCoIn_5$, the Cooper pairing in $PuCoGa_5$ is most probably mediated by antiferromagnetic fluctuations arising from proximity to an antiferromagnetic/paramagnetic border.

It thus appears that $PuCoGa_5$ establishes continuity in the spectrum of energy scales controlling unconventional superconductivity in other *f*-electron systems and in the copper oxides, and that a universal tunable magnetic pairing mechanism may be operative in all materials with functional elements of both localized and itinerant electrons. This leads naturally to the speculation that there may be other materials classes in which antiferromagnetic fluctuations create an exotic form of superconductivity. □

Methods

Spin lattice relaxation and Knight shift analysis

There are several nuclei in $PuCoGa_5$ that can be investigated by NMR: ^{69}Ga ($I = 3/2$), ^{71}Ga ($I = 3/2$), and ^{59}Co ($I = 7/2$). The nuclear hamiltonian is given by $\hat{H} = \gamma h\hat{I}\mathbf{B}_0(1 + K_{tot}) + h\nu_c[3\hat{I}_z^2 - \eta(\hat{I}_x^2 - \hat{I}_y^2)]$, where h is Planck's constant, γ is the gyromagnetic ratio, $\mathbf{B}_0$ is the external magnetic field, $\nu_c = eQV_{cc}/20$, $\eta = (V_{aa} - V_{bb})/V_{cc}$, Q is the quadrupolar moment and the V values are the components of the electric field gradient tensor. In the $PuCoGa_5$ structure (Fig. 2 inset) (space group *P4/mmm*), the Co (1b site) lies directly below and above each Pu, has axial symmetry, and experiences an electric field gradient given by $^{59}\nu_Q = 1.70$ MHz, $\eta = 0$. There are two different ^{69,71}Ga sites: Ga(1) (1c site) and Ga(2) (4*i* site). The Ga(1) site has axial symmetry, has four nearest-neighbour Pu atoms, and experiences a large electric field gradient: $^{69}\nu_Q = 28.28$ MHz, $\eta = 0$. For the Knight shift measurements, both the central line ($I_z = -1/2 \leftrightarrow +1/2$) of the Co and the upper satellite of the ^{71}Ga ($I_z = +3/2 \leftrightarrow +1/2$) were measured. The resonance frequencies f of these transitions can be written in second-order perturbation theory (because $\gamma\mathbf{B}_0 \gg \nu_Q$) by:

$$^{59}f = {}^{59}\gamma\mathbf{B}_0(1 + K) + 15\times{}^{59}\nu_Q^2/(16\times{}^{59}\gamma\mathbf{B}_0)[1 - 10\cos^2(\theta) + 9\cos^4(\theta)] \quad (1)$$

$$^{71}f = {}^{71}\gamma\mathbf{B}_0(1 + K) + {}^{71}\nu_Q(1 - 3\cos(2\theta))/4 + 3\times{}^{71}\nu_Q^2/(2\times{}^{71}\gamma\mathbf{B}_0)\cos^2(\theta)\sin^2(\theta) \quad (2)$$

where θ is the angle between $\mathbf{B}_0$ and the *c* axis of the crystal. T_1^{-1} was measured at the zero-field quadrupolar transition ($I_z = \pm 3/2 \leftrightarrow \pm 1/2$) of the ^{69}Ga(1) by fitting the time dependence of the magnetization recovery after inversion of the nuclear polarization. Sample A, used to measure K_s, was a single crystal oriented with the *c* axis 74.3° from the applied field (8 T) and was measured six months after its growth. Because of radiation damage, the T_c of sample A was reduced from its as-grown value of 18.5 K and in the measuring field of 8 T was ~16 K. Sample B, used to measure T_1^{-1}, consisted of an unoriented powder that had aged two weeks, with $T_c \approx 18.5$ K. Each sample was encapsulated inside an NMR solenoid coil embedded in Stycast epoxy. Thermal contact to the sample was established via gas transfer through stainless steel frits with 2-μm pore sizes located along the axis of the coil.

In the superconducting state, there is a third contribution to the total shift: $-\Delta B/B_0$, where ΔB (the demagnetization field) measures the reduction in the internal magnetic induction due to the diamagnetic shielding currents induced by the applied field. By measuring two different sites (^{59}Co and ^{71}Ga(1)) in $PuCoGa_5$, we determine $\Delta B \approx 40$ Oe at 4 K (ref. 9). Because of the field orientation in our experiment, we can rule out a spin-triplet pairing state with a **d**-vector pointing along the crystallographic *c* axis, as proposed for the spin-triplet superconductors Sr_2RuO_4 and UPt_3 (ref. 12).

For the theoretical fits we modelled the temperature dependence of the strong-coupling superconducting gap function as $\Delta T = \Delta\tanh[b(T_c/T - 1)^{0.5}]$. The ratio of the specific-heat jump to C_N (the normal-state specific heat at T_c) constrained the phenomenological parameters Δ and b as follows: $\Delta C/C_N = (b\Delta/(\pi k_BT_c))^2/(2a)$, with $a = 2/3$ for a free-electron gas. Our choice of parameters $\Delta/k_BT_c = 4$ and $b = 1.74$ lead to a moderately enhanced coefficient $a \approx 1.1$–1.7 for $\Delta C/C_N \approx 1.43$–$2.28$, consistent with reported values for the Sommerfeld coefficient $\gamma_s = C_N/T$ for $T \to 0$ (refs 4, 23).

The spin lattice relaxation and spin susceptibility data were fitted to:

$$T_1^{-1}(T)/T_n^{-1} = -2(T/T_c)\int_0^\infty dE[N^2(E) + M^2(E)]/N_F^2\, df(E)/dE \quad (3)$$

$$\chi_s(T)/\chi_n = -2(T/T_c)\int_0^\infty dE N(E)/N_F df(E)/dE \quad (4)$$

where $f(E)$ is the Fermi–Dirac function, N_F is the density of states at E_F, T_n^{-1} is the normal state relaxation rate at T_c, and $M(E)$ is the 'anomalous' density of quasiparticle states, which vanishes for *d*-wave superconductors. The 'dirty' *d*-wave calculation (assuming a finite density of states from impurities) in Fig. 3a assumes strong impurity scattering in the SCTA with $\Gamma^B/\Delta = 0.01$, $\Delta/k_BT_c = 4$ and $b = 1.74$. Note that it is not possible to fit both the suppression of the Hebel–Slichter coherence peak just below T_c and the linear low-temperature behaviour with an isotropic *s*-wave pairing model, even when magnetic impurity scattering is included.

The normal-state relaxation rate data shown in Fig. 3b have been normalized to the value at $1.25T_c$ in order to avoid complications associated with the pseudogap effect, which suppresses T_1^{-1} in the normal state just above T_c in the copper oxides[14]. There is a qualitative difference between the conventional and the *d*-wave superconductors below and above T_c. For the *d*-wave superconductors, the relaxation rate is given by a single scaling function $f(T/T_c)$ up to at least $3T_c$.

Received 3 September 2004; accepted 4 February 2005; doi:10.1038/nature03428.

1. Monthoux, P. *et al.* Toward a theory of high-temperature superconductivity in the antiferromagnetically correlated cuprate oxides. *Phys. Rev. Lett.* **67,** 3448–3451 (1991).
2. Moriya, T. & Ueda, K. Spin fluctuation spectra and high temperature superconductivity. *J. Phys. Soc. Jpn* **63,** 1871–1880 (1994).
3. Mathur, N. D. *et al.* Magnetically mediated superconductivity in heavy fermion compounds. *Nature* **394,** 39–43 (1998).
4. Sarrao, J. L. *et al.* Plutonium-based superconductivity with a transition temperature above 18 K. *Nature* **420,** 297–299 (2002).
5. Anderson, P. W. Further consequences of symmetry in heavy-electron superconductors. *Phys. Rev. B* **32,** 499 (1985).
6. Petrovic, C. *et al.* Heavy–fermion superconductivity in $CeCoIn_5$ at 2.3K. *J. Phys. Condens. Matter* **13,** L337–L342 (2001).
7. Ohsugi, S. *et al.* Nuclear relaxation in strong coupling superconductors — a comparison with high-T_c superconductors. *J. Phys. Soc. Jpn* **61,** 3054–3057 (1992).
8. Masuda, Y. & Redfield, A. G. Nuclear spin-lattice relaxation in superconducting aluminium. *Phys. Rev.* **125,** 159–163 (1962).
9. Stenger, V. A. *et al.* Nuclear magnetic resonance of A_3C_{60} superconductors. *Phys. Rev. Lett.* **74,** 1649–1652 (1995).
10. Ueda, K. *et al.* ^{29}Si Knight shift in the heavy-fermion superconductor $CeCu_2Si_2$. *J. Phys. Soc. Jpn* **56,** 867–870 (1987).

11. Kotegawa, H. *et al.* Evidence for strong-coupling *s*-wave superconductivity in MgB_2: ^{11}B NMR study. *Phys. Rev. Lett.* **87,** 127001 (2001).
12. Ishida, K. *et al.* Spin-triplet superconductivity in Sr_2RuO_4 identified by ^{17}O Knight shift. *Nature* **396,** 658–660 (1998).
13. Wolfer, W. G. Radiation effects in plutonium. *Los Alamos Sci.* **26,** 274–285 (2000).
14. Kitaoka, Y. *et al.* Nuclear relaxation and Knight shift studies of copper in $YBa_2Cu_3O_{7-y}$. *J. Phys. Soc. Jpn* **57,** 30–33 (1988).
15. Kohori, Y. *et al.* NMR and NQR studies of the heavy fermion superconductors $CoTIn_5$ (T = Co and Ir). *Phys. Rev. B* **64,** 134526 (2001).
16. Ishigaki, A. & Moriya, T. Nuclear magnetic relaxation around the magnetic instability in metals. *J. Phys. Soc. Jpn* **65,** 3402–3403 (1996).
17. Bauer, E. D. *et al.* Structural tuning of unconventional superconductivity in $PuMGa_5$ (M = Co, Rh). *Phys. Rev. Lett.* **93,** 147005 (2004).
18. Moriya, T. & Ueda, K. Antiferromagnetic spin fluctuations and superconductivity. *Rep. Prog. Phys.* **66,** 1299–1341 (2003).
19. Bang, Y. *et al.* T_1^{-1}in the d-wave superconducting state with coexisting antiferromagnetism. *Phys. Rev. B* **69,** 014505 (2004).
20. Hirschfield, P. J. *et al.* Consequences of resonant impurity scattering in anisotropic superconductors: thermal and spin properties. *Phys. Rev. B* **37,** 83–97 (1988).
21. Abrikosov, A. A. *et al. Methods of Quantum Field Theory in Statistical Physics* Ch. 7, Sec. 39.3 (Dover, New York, 1975).
22. Bang, Y. *et al.* Possible pairing mechanisms of $PuCoGa_5$ superconductor. *Phys. Rev. B* **70,** 104512 (2004).
23. Opahle, I. & Oppeneer, P. M. Superconductivity caused by the pairing of plutonium 5f electrons in $PuCoGa_5$. *Phys. Rev. Lett.* **90,** 157001 (2003).
24. Colineau, E. *et al.* Magnetic and electronic properties of the antiferromagnet $NpCoGa_5$. *Phys. Rev. B* **69,** 184411 (2004).
25. Griveau, J. C. *et al.* Pressure dependence of the superconductivity in $PuCoGa_5$. *J. Magn. Magn. Mater.* **272/76,** 154–155 (2004).
26. Savrasov, S. Y. & Kotliar, G. Ground state theory of δ-Pu. *Phys. Rev. Lett.* **84,** 3670–3673 (2000).
27. Kawasaki, Y. *et al.* Anisotropic spin fluctuations in heavy-fermion superconductor $CeCoIn_5$: In-NQR and Co-NMR studies. *J. Phys. Soc. Jpn* **72,** 2308–2311 (2003).

Supplementary Information accompanies the paper on **www.nature.com/nature**.

Acknowledgements We thank Z. Fisk, D. Pines and C. P. Slichter for discussions. This work was performed at Los Alamos National Laboratory under the auspices of the US Department of Energy Office of Science. Y.B. is supported by KOSEF through CSCMR.

Competing interests statement The authors declare that they have no competing financial interests.

Correspondence and requests for materials should be addressed to N.J.C. (curro@lanl.gov).

Two-dimensional spectroscopy of electronic couplings in photosynthesis

Tobias Brixner[1], Jens Stenger[1], Harsha M. Vaswani[1], Minhaeng Cho[2], Robert E. Blankenship[3] & Graham R. Fleming[1]

[1]*Department of Chemistry, and the Institute for Quantitative Biomedical Research (QB3), University of California, Berkeley, and Physical Biosciences Division, Lawrence Berkeley National Laboratory, Berkeley, California 94720, USA*
[2]*Department of Chemistry and Center for Multidimensional Spectroscopy, Division of Chemistry and Molecular Engineering, Korea University, Seoul 136-701, Korea*
[3]*Department of Chemistry and Biochemistry, Arizona State University, Tempe, Arizona 85287, USA*

Time-resolved optical spectroscopy is widely used to study vibrational and electronic dynamics by monitoring transient changes in excited state populations on a femtosecond timescale[1]. Yet the fundamental cause of electronic and vibrational dynamics—the coupling between the different energy levels involved—is usually inferred only indirectly. Two-dimensional femtosecond infrared spectroscopy based on the heterodyne detection of three-pulse photon echoes[2–7] has recently allowed the direct mapping of vibrational couplings, yielding transient structural information. Here we extend the approach to the visible range[3,8] and directly measure electronic couplings in a molecular complex, the Fenna–Matthews–Olson photosynthetic light-harvesting protein[9,10]. As in all photosynthetic systems, the conversion of light into chemical energy is driven by electronic couplings that ensure the efficient transport of energy from light-capturing antenna pigments to the reaction centre[11]. We monitor this process as a function of time and frequency and show that excitation energy does not simply cascade stepwise down the energy ladder. We find instead distinct energy transport pathways that depend sensitively on the detailed spatial properties of the delocalized excited-state wavefunctions of the whole pigment–protein complex.

The Fenna–Matthews–Olson (FMO) bacteriochlorophyll *a* (BChl) protein of green sulphur bacteria serves both as an antenna for collecting light energy and as a mediator for directing light excitations from the chlorosome antenna to the reaction centre[9–12]. The FMO protein is a trimer of identical subunits, each containing seven BChl pigments. Because of its comparatively simple structure it is often employed as a model system for excitonic (delocalization) effects in photosynthesis research[13]. However, it is not clear to what extent individual spectral features, such as those in the linear FMO absorption spectrum, are caused by differences in site energies (arising from the interaction of the BChl pigments with their local protein environment) or by energy splitting from excitonic coupling (that is, pigment–pigment interaction)[14–16]. With two-dimensional femtosecond spectroscopy, couplings can be made visible directly.

Two-dimensional (2D) optical spectroscopy[3,8,17–21] measures the full nonlinear polarization of a quantum system in third order with respect to the field–matter interaction[3,8,22]. A sequence of three ultrashort laser pulses excites the sample, and the emitted phase-matched signal field is detected in amplitude and phase as a function of optical frequency and the three experimentally controlled excitation-pulse time delays τ, T and t. Fourier transforms of the data[8,21] reveal complex-valued 2D (ω_τ, ω_t) frequency maps of the system's response, where ω_τ and ω_t are the conjugate Fourier frequencies of τ and t. The real part can be interpreted as the transient field amplitude at a particular probe frequency ω_t, induced by a specific excitation frequency ω_τ, after the waiting time (population time) T. The imaginary part describes transient changes in the refractive index. Whereas diagonal peaks in the 2D traces correspond to linear absorption positions, any off-diagonal contributions indicate coupling and, for $T > 0$, energy transfer. In the infrared regime, 2D maps for vibrational couplings have been determined[2,4–7], yielding transient structural information. Two-colour photon-echo spectroscopy has been used to study electronic coupling in a homodimer[23], but molecular cross-peak features for electronic transitions in the visible range have not yet been reported.

The experimental 2D trace of the FMO complex for $T = 0$ fs is shown in Fig. 1a. The positions of the three main diagonal peaks match the linear absorption spectrum below (Fig. 1d, solid black line). Elongation of these features along the diagonal indicates a correlation between excitation and emission frequencies within the same pigment and hence inhomogeneous spectral broadening[2,24,25]. Analysis of the 2D contour shapes can recover the homogeneous linewidths. More importantly, however, several off-diagonal features (positive and negative) are clearly visible. Using an assignment of exciton levels (horizontal and vertical lines numbered 1–7 in Fig. 1a), one can qualitatively identify the extent of mutual correlations as the magnitude of the corresponding cross peaks. Quantitative evaluation is done by comparison with simulations as shown below. The cross-peak amplitude is determined by quantum-mechanical interference from different nonlinear optical transition pathways. Because of the electronic coupling between pigments, the excitonic transition dipoles become linear combinations of pigment